Nonlinear constructive interference in electrical lattices

H. S. Bhat*
School of Natural Sciences, University of California, P. O. Box 2039, Merced, California 95344, USA

E. Afshari†
Electrical and Computer Engineering, Cornell University, Ithaca, New York 14853, USA

(Received 29 November 2007; revised manuscript received 1 April 2008; published 6 June 2008)

We analyze the constructive interference of input signals in nonlinear, discrete, two-dimensional media. The media consist of inductor-capacitor lattices with saturating, voltage-dependent capacitors. We find that nonlinearity significantly boosts the ability of such media to generate large-amplitude output signals from small-amplitude inputs. To understand this boosting, we develop a general perturbative method suitable for finding the steady-state solution of a damped $N \times N$ nonlinear lattice that is driven at a single frequency. We verify our theory using extensive numerical simulations.

DOI: 10.1103/PhysRevE.77.066602 PACS number(s): 05.45.Yv, 84.40.Az, 63.20.Pw

I. INTRODUCTION

Consider a square, two-dimensional lattice of inductors and capacitors as shown in Fig. 1. Suppose that a sinusoidal voltage V of amplitude A is applied along the left and bottom edges. The boundary forcing produces two incident waves of equal amplitude A that collide at a right angle and produce an outgoing wave with amplitude A_R. If the capacitors are voltage independent, the lattice dynamics are linear. Assuming the inputs are all in phase and that they all have equal amplitude A, we find at a fixed time $T>0$ that the peak output voltage is equal to mA for some positive number m that does not depend on A. This is the meaning of linearity: if we double the amplitudes of all the inputs, we expect the outputs to also double in amplitude.

If, however, the capacitors are voltage dependent, the lattice dynamics are nonlinear. For in-phase, equal-amplitude inputs, the peak output amplitude A_R at a fixed time $T>0$ will depend nonlinearly on the input amplitude A. What we show in this paper is that nonlinearity causes a significant boost in the peak output. For a specific choice of capacitance function $C(V)$, we find that the nonlinear output A_R can be several times the linear output mA. It turns out that A_R is limited only by the saturation voltage of the capacitors, the size of the lattice, and the final time T.

We call this phenomenon nonlinear constructive interference. To analyze this interference, we break the overall problem into a sequence of smaller problems. The dynamics of the smallest 1×1 block is governed by a single damped, driven, nonlinear oscillator equation. Given a specific capacitance function $C(V)$, the nonlinear oscillator equation may be analyzed perturbatively, producing analytical approximations for the output of each stage. We find that nonlinearity boosts the amplitude of the output signal by increasing its frequency content. We find that in spite of approximations made along the way, our perturbative results for 1×1 and 2×2 lattices are in detailed quantitative agreement with numerical results. We generalize the perturbative method to the case of an $N \times N$ lattice with N arbitrary, and we claim that increasing the size of the lattice strengthens the higher harmonics that are induced by single-frequency boundary forcing. Our expectation is that regardless of the amplitudes of the input signals, we can find a sufficiently large lattice where the peak output amplitude is bounded only by capacitor saturation.

In studying this problem, we are motivated by both applications and theoretical concerns. Prior work on linear, two-dimensional inductor-capacitor lattices [1–3] has demonstrated their utility in analog applications, including a power amplifier and a Fourier transform device. These two-dimensional (2D) lattices can be fabricated on silicon using standard complementary metal-oxide–semiconductor (CMOS) processes. Compared with other silicon-based solutions, the lattice approach features a high cutoff frequency, high throughput, and low latency. By explaining how nonlinear 2D LC lattices can nonlinearly combine the amplitudes of input signals, we take a first step toward actually using such lattices for on-chip microwave signal generation and processing.

Spatially discrete systems similar to the one investigated in this paper have been of recent interest to theorists as well. For 2D nonlinear mass-spring lattices of Fermi-Pasta-Ulam (FPU) type, several authors [4,5] have proven the existence of discrete solitary waves. The link between FPU and inductor-capacitor lattices has been exploited [6,7] to show the existence of discrete breathers for both rectangular and hexagonal versions of both types of lattices. Aside from these types of systems, there has been a tremendous amount of work on 2D discrete nonlinear Schrödinger (DNLS) systems, which we do not attempt to survey here.

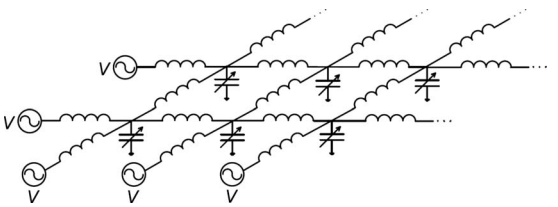

FIG. 1. Two-dimensional nonlinear transmission lattice.

*hbhat@ucmerced.edu
†ehsan@ece.cornell.edu

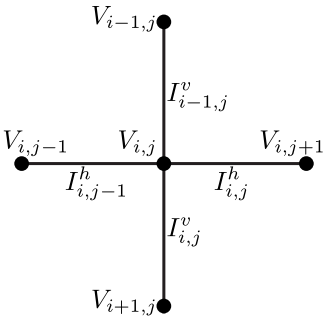

FIG. 2. Node and edge numbering for Kirchhoff's laws (1a)–(1c).

Most of the literature on spatially discrete nonlinear waves does not deal with the effects of forcing and dissipation. Notable exceptions include the dynamics of arrays of Josephson junctions (discrete sine-Gordon lattices) [8–12] as well as discrete Klein-Gordon and Frenkel-Kontorova lattices [13–16], where damping and driving have been examined extensively. These papers focus on mathematically interesting properties such as chaos, synchronization, and the existence and stability of coherent structures such as solitons, kinks, and breathers. To our knowledge, none of these prior works examines nonlinear constructive interference in a spatially discrete system.

II. PRELIMINARY NUMERICAL EXPERIMENT

To give the reader a concrete idea of what we mean by nonlinear interference, we first describe a numerical solution of Kirchhoff's laws on the lattice. We use the node and edge numbering as given in Fig. 2. Let V denote voltage, and let $I^{h,v}$ denote, respectively, horizontal and vertical current. All three of these quantities are $N\times N$ matrices. Then Kirchhoff's laws are

$$\frac{d}{dt}[Q_{i,j}] = I^h_{i,j-1} - I^h_{i,j} + I^v_{i,j} - I^v_{i-1,j}, \quad 1 \le i,j \le N, \tag{1a}$$

$$L\frac{d}{dt}I^v_{i,j} = V_{i+1,j} - V_{i,j}, \quad 1 \le i,j \le N, \tag{1b}$$

$$L\frac{d}{dt}I^h_{i,j} = V_{i,j} - V_{i,j+1}, \quad 1 \le i \le N, \quad 0 \le j \le (N-1). \tag{1c}$$

Here the inductance L and capacitance function $C(V)$ are taken to be uniform throughout the lattice. We use $Q_{i,j} = Q(V_{i,j})$ to denote the charge stored in the nonlinear capacitor that connects node (i,j) to ground. For nonlinear capacitors, the charge is related to the capacitance by $dQ_{i,j} = C(V_{i,j})dV_{i,j}$.

In (1a), we use the convention $I^v_{0,j} = I^h_{i,N} = 0$ to handle the $i=1$ and $j=N$ cases. In (1), when $i=N$ we treat $V_{N+1,j}(t)$ as a prescribed source and forcing function. Similarly, when $j=0$ in (1c), we treat $V_{i,0}(t)$ as a prescribed source and forcing function.

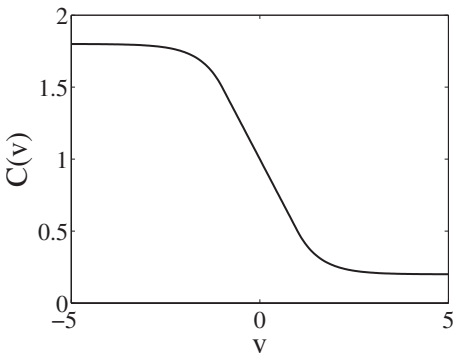

FIG. 3. Voltage-dependent capacitance $C(v)$ as defined in (2), with $C_0=1$, $b=0.25$, $\alpha=0.5$, and $\gamma=1.66$.

It is instructive to carry out the differentiation on the left-hand side of (1a). Let $v(t)$ denote $V_{ij}(t)$, let overdots denote differentiation with respect to t, and let primes denote differentiation with respect to v. Then we obtain $d/dt[Q_{i,j}] = Q'(v)\dot{v} = C(v)\dot{v}$, so that (1a) may be rewritten as

$$\frac{d}{dt}V_{i,j} = \frac{I^h_{i,j-1} - I^h_{i,j} + I^v_{i,j} - I^v_{i-1,j}}{C(V_{ij})}, \quad 1 \le i,j \le N.$$

A physically meaningful capacitance function will be positive and will also saturate for sufficiently small and sufficiently large voltages. With these qualifications in mind, we choose the voltage-dependent capacitance function

$$C(v) = C_0 \times \begin{cases} \left(\alpha - \frac{4}{5}\right)e^{\gamma(\alpha/(2b)+v)} + \frac{9}{5}, & v \le -\frac{\alpha}{2b}, \\ 1 - 2bv, & |v| < \frac{\alpha}{2b}, \\ \left(\frac{4}{5} - \alpha\right)e^{\gamma(\alpha/(2b)-v)} + \frac{1}{5}, & v \ge \frac{\alpha}{2b}. \end{cases} \tag{2}$$

Note that the parameter b is a measure of the voltage dependence of this capacitance function. As b approaches zero, the function $C(v)$ approaches the constant function $C(v)=C_0$. Hence b controls the degree to which Eq. (1a) is nonlinear; as $b\to 0$, the dynamics approaches that of a perfectly linear medium. A plot of $C(v)$ is shown in Fig. 3.

For the $N\times N$ lattice, we impose the boundary forcing

$$V_{i,0}(t) = V_{N+1,j}(t) = A \sin t, \quad (N-19) \le i \le N,$$

$$1 \le j \le 20.$$

That is, we apply in-phase, equal-amplitude sinusoidal signals to each of the last 20 nodes on the left side of the lattice, as well as to each of the first 20 nodes on the bottom edge of the lattice. Other boundary nodes are set to zero.

Sweeping through values of the input amplitude A, we numerically solve system (1) with $N=80$. We take $L=1$ and $C(v)$ given by (2) with $C_0=1$, $b=0.25$, $\alpha=0.5$, and $\gamma=1.66$. We stop each simulation at $T=8\pi$ and record the peak output amplitude A_R for $0\le t\le T$. By peak output amplitude, we mean

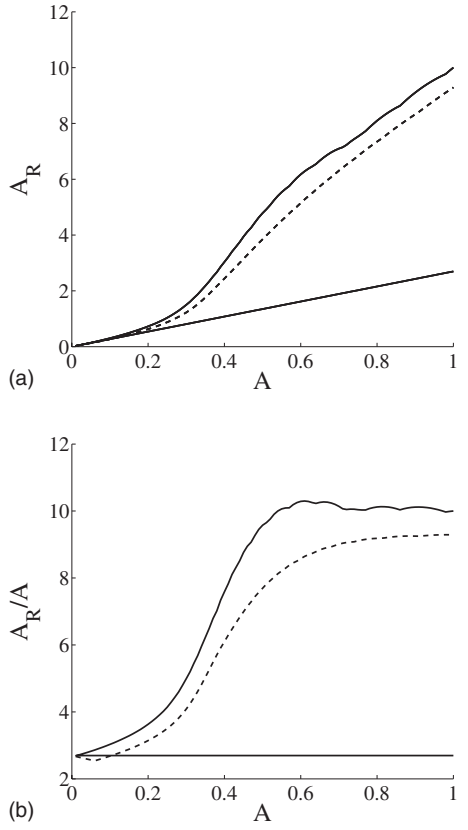

FIG. 4. Output amplitude A_R and boost ratio A_R/A as a function of input amplitude A for an 80×80 lattice. The solid straight lines show results for a linear lattice with constant capacitance $C_0=1$. The curved lines show results for a nonlinear lattice with voltage-dependent capacitance $C(v)$ as shown in Fig. 3. The solid curved line shows the peak output amplitude A_R at $T=8\pi$, while the dashed curved line shows the peak output amplitude A_R' at $T/2=4\pi$. The results show that nonlinearity significantly boosts the peak output voltage, but that the boost ratio is bounded.

$$A_R = \max_{\substack{1\le i,\ j\le N \\ 0\le t\le T}} V_{i,j}(t). \tag{3}$$

Note that the stopping time T is sufficiently small so that the signals have *not* reached very far into the lattice; in particular, the voltage and current at the right and top boundaries are still zero. We carry out the same test on a linear ($b=0$) lattice with $L=1$ and $C(V)=C_0=1$. The results are plotted in Fig. 4.

What these results show is that the voltage dependence of the capacitor significantly boosts the peak output voltage. As one might expect, the larger the input amplitude A, the greater the difference between the peak outputs of the nonlinear and linear systems. The results also show that there is a limit to the boosting effect of nonlinearity: for this particular numerical experiment, the ratio A_R/A reaches a maximum of approximately 10.

In Fig. 4(b), we have also plotted the peak output amplitude A_R' at time $T/2=4\pi$; this quantity is defined just as in (3), but with T replaced by $T/2$ on the right-hand side. Figure 4(b) shows that if we do not run the simulation long enough, then for very small input amplitudes—say, $0<A<0.1$—there is a possibility that nonlinearity causes a small decrease in the boost ratio A_R/A; see the portion of the dashed curve that lies below the straight linear boost line. Because this effect disappears if we take the peak amplitude at $T=8\pi$ instead of $T=4\pi$, it must be a transient effect; in the present work, we are concerned with steady-state nonlinear interference and transient effects will not be considered.

The natural question to ask at this stage is, why and how do voltage-dependent capacitors boost the output amplitude? An ideal answer to this question would involve the full solution of Kirchhoff's laws subject to the driving and damping described above. For an 80×80 lattice, there are 6400 unknown voltages and 12 800 unknown currents. The ideal answer would involve solving a nonautonomous, nonlinear dynamical system in $\mathbb{R}^{19200}$, a rather daunting task. A natural approach would be to pass to a continuum limit and derive a single partial differential equation (an infinite-dimensional system) that approximates the dynamics of the 80×80 lattice. For reasons described at the end of this paper, that is not the strategy we take here.

Our approach will be to deal directly with the $N\times N$ spatially discrete system. We caution the reader that we do not at this time have an analytical model that generates the curves in Fig. 4. Our goal is instead to explain how such curves are possible—i.e., how it is possible that introducing voltage-dependent capacitors can dramatically boost the observed lattice voltages. Along the way, we present an analytical method for determining the steady-state output of a nonlinear lattice of arbitrary size. To accomplish this, we take a careful look at 1×1 and 2×2 lattices.

III. PERTURBATIVE ANALYSIS

We theorize that the macroscopic dynamics of the whole lattice can be understood by appropriately scaling the microscopic dynamics of a very small part of the lattice. Our strategy will be to obtain detailed information about the dynamics of the bottom-left corner of the lattice and then use this information to infer properties of the 80×80 lattice. To keep the algebra simple, we assume that the voltages in our problem are sufficiently close to zero so that $C(v)=C_0(1-2bv)$. At the voltage v, the charge stored in the capacitor is given by $Q(v)=\int C(v)dv=C_0(v-bv^2)$.

A. Steady-state solution for the 1×1 lattice

We examine the bottom-left corner of the lattice from Fig. 1. By treating the rest of the lattice as a resistive load, we obtain the circuit diagrammed in Fig. 5. In this model, the lower-left corner interacts with the rest of the lattice through the load R. Kirchhoff's laws of voltage and current for this circuit are

$$V_1 - V_R = L\frac{d}{dt}I_1, \tag{4a}$$

$$V_2 - V_R = L\frac{d}{dt}I_2, \tag{4b}$$

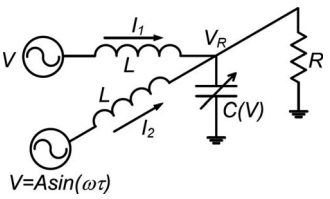

FIG. 5. The bottom-left corner of the nonlinear 2D LC lattice shown in Fig. 1, with the rest of the lattice treated as a resistive load R.

$$I_1 + I_2 - \frac{V_R}{R} = C_0 \frac{d}{dt}(V_R - bV_R^2). \tag{4c}$$

Here V_1 and V_2 are the inputs from the boundary and V_R is the output. Note that if $V_1(t)=V_2(t)$, then (4a) and (4b) imply that $I_1(t)=I_2(t)$. In this case, we denote $I(t)=I_j(t)$. Differentiating (4c), we obtain

$$LC_0 \frac{d^2}{dt^2}(V_R - bV_R^2) + \frac{L}{R}\frac{d}{dt}V_R + 2V_R = 2V. \tag{5}$$

This is a damped, driven nonlinear oscillator equation. We introduce the nondimensionalized time variable $\tau=t/\sqrt{LC_0}$ and the change of variable $V_R(t)=W(\tau)$. Let overdots denote differentiation with respect to τ. With these changes, (5) becomes

$$\ddot{W} - 2b\dot{W}^2 - 2bW\ddot{W} + K\dot{W} + 2W = 2S, \tag{6}$$

with $K=\sqrt{L/C_0}/R$ as a nondimensional parameter and $S(\tau):=V(\sqrt{LC_0}\tau)$.

We are interested in the case where at $\tau=0$, the voltage and current in the circuit are zero—i.e., $W(0)=0$ and $\dot{W}(0)=0$. Then, at $\tau=0$, a sinusoidal input voltage is switched on:

$$S(\tau) = A\ \sin(\omega\tau)H(\tau), \tag{7}$$

where $\omega=\Omega\sqrt{LC_0}$ is a nondimensionalized frequency and $H(\tau)$ is the Heaviside unit step function,

$$H(\tau) = \begin{cases} 1, & \tau \geq 0, \\ 0, & \tau < 0. \end{cases}$$

Since (6) is nonlinear, we cannot claim that the solution W for this choice of S will be a simple superposition of transient and steady-state pieces. Still, we expect that $W(\tau)$ gradually decays and deforms from a transient solution (near $\tau=0$) into a steady-state solution (as $\tau\to+\infty$). Let us make the simplifying assumption that W reaches steady state very quickly. This assumption will later be justified using numerics. For now, we focus on obtaining a steady-state solution to (6). To do this, we pretend as if the input voltage was switched on at $\tau=-\infty$. That is, we take $S(\tau)$ to be

$$S(\tau) = A\ \sin(\omega\tau). \tag{8}$$

We now proceed to perturbatively solve (6) with S given by (8).

When $b=0$ in (6), W satisfies a damped, driven harmonic oscillator equation. The driving is given by $\hat{V}$, and the damping coefficient is K. Since we know how to solve the $b=0$ equation, we expand the solution $W(\tau)$ in a series in b:

$$W(\tau) = W_0(\tau) + bW_1(\tau) + b^2W_2(\tau) + \cdots. \tag{9}$$

The true nonlinear solution should be expressed as $W(T)$ where $T=\tau(1+b\beta_1+b^2\beta_2+\cdots)$, but for our purposes, it will turn out that ignoring this frequency shift yields a perfectly useable approximation. Inserting (9) into (6), we find that the $O(b^0)$ equation is

$$\ddot{W}_0 + K\dot{W}_0 + 2W_0 = 2A\ \sin(\omega\tau). \tag{10}$$

As mentioned above, we seek the steady-state solution of this equation. This can be done in an elegant way by taking the Fourier transform of both sides. In what follows, α is the frequency variable that is Fourier conjugate to time τ:

$$(-\alpha^2 + i\alpha K + 2)\hat{W}_0(\alpha) = \frac{A}{i}\delta(\alpha-\omega) - \frac{A}{i}\delta(\alpha+\omega).$$

This yields

$$\hat{W}_0(\alpha) = \frac{A}{-i\alpha^2 - K\alpha + 2i}\delta(\alpha-\omega) + \frac{A}{i\alpha^2 + K\alpha - 2i}\delta(\alpha+\omega).$$

Now taking the inverse Fourier transform of both sides gives

$$W_0(\tau) = Be^{i\omega\tau} + B^*e^{-i\omega\tau}, \tag{11}$$

$$B = \frac{A}{-i\omega^2 - K\omega + 2i}. \tag{12}$$

Using (9), we may write the $O(b^1)$ equation from (6):

$$\ddot{W}_1 + K\dot{W}_1 + 2W_1 = 2\dot{W}_0^2 + 2W_0\ddot{W}_0 = (-2B^2\omega^2e^{2i\omega\tau}) + \text{c.c.}, \tag{13}$$

where we used (11) to evaluate the right-hand side of (13). Examining (13), we find that it is once again a damped, driven harmonic oscillator equation. We ignore the transient part of the solution. We may write the steady-state solution as

$$W_1(\tau) = Ce^{2i\omega\tau} + \text{c.c.}, \tag{14}$$

$$C = \frac{4\omega^2B^2}{4\omega^2 - 2iK\omega - 2}. \tag{15}$$

Finally, we use (9) to write the $O(b^2)$ equation from (6):

$$\begin{aligned}\ddot{W}_2 + K\dot{W}_2 + 2W_2 &= 4\dot{W}_0\dot{W}_1 + 2W_1\ddot{W}_0 + 2W_0\ddot{W}_1 \\ &= (-18BC\omega^2e^{3i\omega\tau} - 2B^*C\omega^2e^{i\omega\tau}) + \text{c.c.}\end{aligned} \tag{16}$$

Note that we used (11) and (14) to evaluate the right-hand side of (16). Again, ignoring transients, we write the steady-state solution as

$$W_2(\tau) = D_1e^{3i\omega\tau} + D_2e^{i\omega\tau} + \text{c.c.}, \tag{17}$$

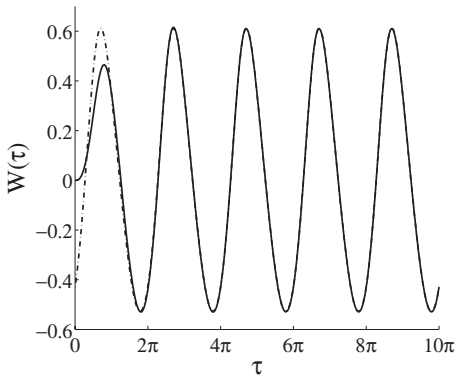

FIG. 6. The solid black curve is the numerical solution $W^{\mathrm{num}}(\tau)$ of (4) with saturating capacitance (2). The dashed black curve is the perturbative solution $W(\tau)$ from (19). Note that the numerical solution reaches steady state very quickly and also that both solutions agree very well for $\tau \geq 2\pi$. Both solutions have the same parameters $A=0.4$, $\omega=1$, $K=1$, and $b=0.25$.

$$D_1 = \frac{-18BC\omega^2}{-9\omega^2 + 3iK\omega + 2}, \quad D_2 = \frac{-2B^*C\omega^2}{-\omega^2 + iK\omega + 2}. \tag{18}$$

Putting (11), (14), and (17) together, one arrives at the following $O(b^2)$ approximation to the steady-state solution of (6):

$$W(\tau) = Be^{i\omega\tau} + bCe^{2i\omega\tau} + b^2D_1e^{3i\omega\tau} + b^2D_2e^{i\omega\tau} + \text{c.c.} \tag{19}$$

The coefficients B, C, D_1, and D_2 depend on A, ω, and K, but they do not depend on b.

B. Numerics for the 1×1 lattice

Earlier we claimed that the true solution of (4) reaches steady state quickly. To justify this claim, we numerically solve (4) with the capacitance function $C(v)$ given by (2) and forcing function $V_1(t)=V_2(t)=A \sin t$. We take $L=1$, $C_0=1$, $b=0.25$, $R=1$, and $A=0.4$. With this choice of constants, we see that $\tau=t$, $\omega=1$, and $K=1$. Let us denote the numerical solution for the output voltage by $W^{\mathrm{num}}(\tau)$. (This voltage is labeled as V_R in our earlier Fig. 5.)

We plot $W^{\mathrm{num}}(\tau)$ as the solid black curve in Fig. 6. It is clear that $W^{\mathrm{num}}(\tau)$ reaches steady state very quickly; for $\tau \geq 2\pi$, after just one period of input forcing, there is no discernable transient behavior.

Also in Fig. 6 we plot using a dash-dotted curve the perturbative steady-state solution $W(\tau)$ given by (19). From $\tau=2\pi$ until $\tau=8\pi$, both the solid and dash-dotted curves agree extremely well.

Finally, note that the choice of $C(v)=C_0(1-2bv)$ implicit in (6) is equivalent to $C(v)$ defined earlier by (2) and Fig. 3, as long as the voltage v satisfies $|v| \leq \alpha/(2b)=1.0$. As shown in Fig. 6, this condition is satisfied for both the numerical and perturbative solutions.

C. Interpretation

It is clear from our derivation of (19) that going from the $O(b^k)$ approximation to the $O(b^{k+1})$ approximation results in the addition of higher harmonics to the solution. Driving the nonlinear oscillator Eq. (6) at a single frequency as in (8) yields a solution with frequency content consisting of multiples of the original frequency. Note also that setting $b=0$ in (19) removes all of the higher harmonics; this shows that the steady-state response for the linear, constant capacitor system is $2|B|$ where B is defined by (12).

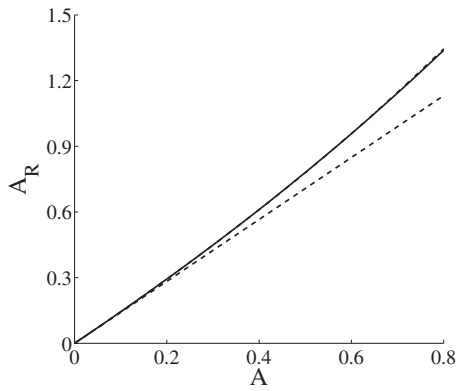

FIG. 7. There are three curves plotted here, all of which give steady-state output amplitude A_R as a function of input amplitude A for the 1×1 lattice with $\omega=1$ and $K=1$. The two upper curves (indistinguishable except when A is close to 0.8) are for a nonlinear lattice with $b=0.25$, while the lower line (in black dashes) is for a linear lattice with $b=0$. The solid black and dash-dotted upper curves were generated, respectively, by using numerical simulation of (4) and the perturbative approximation (19). Note that when $A=0.4$, the nonlinear amplitude is 8% larger than the linear amplitude; when $A=0.8$, the difference is 19%.

We claim that for $b>0$, the higher harmonics add constructively to the amplitude. To show that this is the case, we use (19) to plot the maximum output amplitude A_R as a function of the input amplitude A for the case where $\omega=1$, $K=1$, and $b=0.25$. Here A_R is defined as

$$A_R = \max_{\tau\in[0,2\pi]} |W(\tau)|,$$

and this is shown as the dash-dotted black curve in Fig. 7.

We also generate numerical solutions of the output voltage—denoted, as before, by $W^{\mathrm{num}}(\tau)$—of the system (4a)–(4c) with saturating capacitance (2) and forcing $V_1(t)=V_2(t)=A \sin t$ for values of A in the range $0\leq A\leq 0.4$. We run the simulation from $\tau=0$ until $\tau=14\pi$ with the parameters $\omega=1$, $K=1$, and $b=0.25$. We then compute the maximum output amplitude after the numerical solution has reached steady state—i.e.,

$$A_R^{\mathrm{num}} = \max_{\tau\in[10\pi,14\pi]} |W^{\mathrm{num}}(\tau)|.$$

This is shown as the solid black curve in Fig. 7. Note that the solid black curve and dash-dotted black curve agree so closely that they are right on top of one another. The only difference between these two curves appears as A approaches 0.8, at which point there is a small error in the perturbative approximation. Finally, we plot both versions of A_R together with the maximum amplitude that would have been observed had we set $b=0$—i.e., if we had a linear system with constant

capacitors. The maximum amplitude for the linear $b=0$ system is given by the dashed black curve, which in Fig. 7 is strictly below the $b=0.25$ curves.

In the middle of the graph, when $A=0.4$, we have that $A_R=0.6108$ and $A_R^{\text{num}}=0.6103$. The linear response to this input has amplitude 0.5657. When the input amplitude is $A=0.4$, the higher harmonics in the nonlinear $b=0.25$ response provide a total amplitude boost of 8% over the linear response.

D. Frequency response

So far in our numerical simulations we have chosen $L=1$, $C_0=1$, and the input forcing $V(t)=A\sin\omega t$ where $\omega=\sqrt{LC_0}=1$. At this stage, it is natural to ask what happens when we vary the input frequency.

For the linear $b=0$ system, we know that the steady-state response will be given by

$$A_R(\tau)=Be^{i\omega\tau}+B^*e^{-i\omega\tau},$$

with B defined by (12). The amplitude of this signal is given by

$$|B|=\left|\frac{A}{-i\omega^2-K\omega+2i}\right|=\frac{|A|}{\sqrt{4+(-4+K^2)\omega^2+\omega^4}}. \tag{20}$$

A simple calculation shows that $|B|$ is maximized when

$$\omega_r=\pm\sqrt{2-\frac{K^2}{2}}.$$

This frequency ω_r is the *resonant frequency* for the linear $b=0$ case of the oscillator Eq. (6). For $K=1$, this corresponds to $\omega_r=\sqrt{3/2}\approx 1.2247$. The natural question to ask is how nonlinearity affects this resonant frequency. That is, how does the amplitude of the perturbative approximation $W(\tau)$ given by (19) vary as a function of ω?

To answer this question, we plot both the linear $b=0$ amplitude (20) and the maximum nonlinear $b=0.25$ amplitude

$$A_R=\max_{\tau\in[0,2\pi]}|W(\tau)|$$

as functions of ω. We set $A=0.4$ and $K=1$ for this test. The results are shown in Fig. 8. The solid black and dash-dotted curves are, respectively, the frequency response for the nonlinear and linear systems. Two things are clear from this plot. First, the nonlinear response reaches a peak amplitude at a frequency that is very close to the linear resonant frequency ω_r. Second, $\omega=1$ is in the middle of an interval of frequencies where the nonlinear response is significantly higher in amplitude than the linear response. In other words, nonlinearity-driven amplitude boosting is robust with respect to changes in the driving frequency.

We expect that this robustness carries through to the case of 2×2 and, indeed, $N\times N$ lattices. In what follows, we take $\omega=1$ and demonstrate that nonlinear constructive interference does not depend on driving the system at the resonant frequency ω_r.

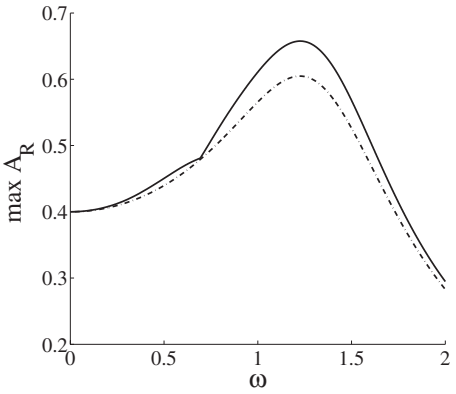

FIG. 8. Frequency response for the linear $b=0$ system (given by the dash-dotted curve) and the nonlinear $b=0.25$ system (given by the solid curve). Both curves gives the maximum amplitude of the output signal A_R as a function of input frequency ω in the case where $K=1$ and $A=0.4$. Here A_R is computed using the steady-state perturbative approximation (19).

E. Steady-state solution for the 2×2 lattice

Next we examine the effect of an additional stage on the amplitude boost. That is, we analyze the 2×2 bottom-left subblock of the original lattice where, once again, the rest of the lattice is treated as a resistive load R. The circuit is diagrammed in Fig. 9(a). In the case of equal-amplitude, in-phase inputs, symmetry allows us to replace this circuit by the equivalent circuit diagrammed in Fig. 9(b). We again ignore capacitor saturation and use $C(v)=C_0(1-2bv)$ and $Q(v)=C_0(v-bv^2)$. Then Kirchhoff's laws for this circuit are

$$\frac{L}{2}\frac{d}{dt}I_1=V-V_1,\quad \frac{L}{2}\frac{d}{dt}I_2=V_1-V_2, \tag{21a}$$

$$\frac{L}{2}\frac{d}{dt}I_3=V-V_2,\quad \frac{L}{2}\frac{d}{dt}I_4=V_2-V_R, \tag{21b}$$

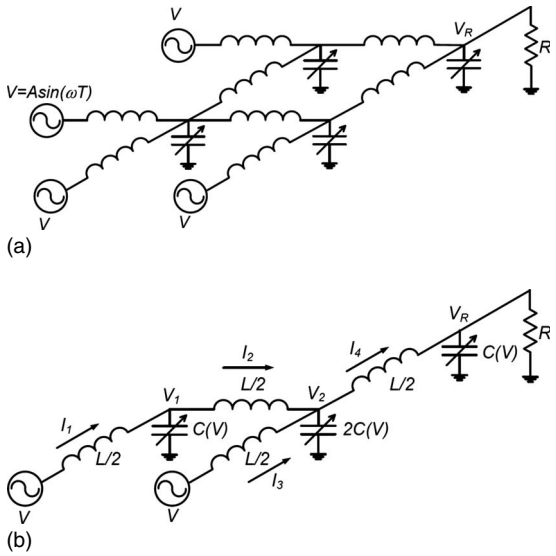

FIG. 9. The 2×2 lower-left corner of the original lattice shown in Fig. 1, with the rest of the lattice treated as a resistive load R.

$$C_0\frac{d}{dt}[V_1 - bV_1^2] = I_1 - I_2, \tag{21c}$$

$$2C_0\frac{d}{dt}[V_2 - bV_2^2] = I_2 + I_3 - I_4, \tag{21d}$$

$$C_0\frac{d}{dt}[V_R - bV_R^2] = I_4 - \frac{V_R}{R}. \tag{21e}$$

Differentiating (21c)–(21e) with respect to t and plugging in (21a) and (21b), we obtain the following system of three coupled nonlinear oscillators:

$$C_0\frac{d^2}{dt^2}[V_1 - bV_1^2] = \frac{2}{L}(V - 2V_1 + V_2), \tag{22a}$$

$$C_0\frac{d^2}{dt^2}[V_2 - bV_2^2] = \frac{1}{L}(V + V_1 - 3V_2 + V_R), \tag{22b}$$

$$C_0\frac{d^2}{dt^2}[V_R - bV_R^2] = \frac{2}{L}(V_2 - V_R) - \frac{1}{R}\frac{d}{dt}V_R. \tag{22c}$$

As in the 1×1 case, we use the nondimensionalized time $\tau = t/\sqrt{LC_0}$ and the change of variables $V_R(t) = W(\tau)$ and $V_j(t) = W_j(\tau)$ for $j = 1,2$. Let primes denote differentiation with respect to τ; then, after changing variables and using the fact that $[x(\tau) - bx(\tau)^2]'' = x'' - 2b(x')^2 - 2bxx''$, system (22) becomes

$$W_1'' + 4W_1 - 2W_2 = 2S + 2bW_1W_1'' + 2b(W_1')^2, \tag{23a}$$

$$W_2'' + 3W_2 - W_1 - W_R = S + 2bW_2W_2'' + 2b(W_2')^2, \tag{23b}$$

$$W_R'' + KW_R' + 2W_R - 2W_2 = 2bW_RW_R'' + 2b(W_R')^2, \tag{23c}$$

where $K = \sqrt{L/C_0}/R$ as a nondimensional parameter and $S(\tau) := V(\sqrt{LC_0}\tau)$. As in the 1×1 case, we may derive a perturbative steady-state solution to (23). First we develop the unknowns as series in b:

$$W_1 = W_1^{(0)} + bW_1^{(1)} + b^2W_1^{(2)} + \cdots, \tag{24a}$$

$$W_2 = W_2^{(0)} + bW_2^{(1)} + b^2W_2^{(2)} + \cdots, \tag{24b}$$

$$W_R = W_R^{(0)} + bW_R^{(1)} + b^2W_R^{(2)} + \cdots. \tag{24c}$$

We plug these expansions into (23). As before, we concern ourselves only with steady-state solutions for single-frequency forcing, so we take

$$S(\tau) = A\,\sin(\omega\tau) = \frac{A}{2i}e^{i\omega\tau} + \text{c.c.} \tag{25}$$

(a) *Obtaining* $\mathbf{W}^{(0)}$ for single-frequency forcing. With $S(\tau)$ given by (25), we now explain how to solve for $\mathbf{W}^{(0)} = (W_1^{(0)}, W_2^{(0)}, W_R^{(0)})^T$. Let M be the matrix

$$M(\alpha) = \begin{pmatrix} -\alpha^2 + 4 & -2 & 0 \\ -1 & -\alpha^2 + 3 & -1 \\ 0 & -2 & -\alpha^2 + iK\alpha + 2 \end{pmatrix}. \tag{26}$$

Let $\hat{\mathbf{W}}^{(k)} = (\hat{W}_1^{(k)}, \hat{W}_2^{(k)}, \hat{W}_R^{(k)})$ denote the Fourier transform of $\mathbf{W}^{(k)}$, and let $\hat{\mathbf{r}}^{(k)}$ denote the vector obtained by taking the Fourier transform of the $O(b^k)$ terms on the right-hand side of (23) after we have plugged in the expansion (24) and the function (25). Then the Fourier transform of the $O(b^0)$ equation reads

$$M\hat{\mathbf{W}}^{(0)} = \hat{\mathbf{r}}^{(0)}. \tag{27}$$

In this case, the $O(b^0)$ term on the right-hand side of (22) is

$$\mathbf{r}^{(0)} = \begin{pmatrix} \frac{A}{i}e^{i\omega\tau} - \frac{A}{i}e^{-i\omega\tau} \\ \frac{A}{2i}e^{i\omega\tau} - \frac{A}{2i}e^{-i\omega\tau} \\ 0 \end{pmatrix},$$

so the Fourier transform (with α as the Fourier conjugate to τ) is

$$\hat{\mathbf{r}}^{(0)} = \begin{pmatrix} \frac{A}{i}\delta(\alpha - \omega) - \frac{A}{i}\delta(\alpha + \omega) \\ \frac{A}{2i}\delta(\alpha - \omega) - \frac{A}{2i}\delta(\alpha + \omega) \\ 0 \end{pmatrix}.$$

From (27) we may then derive

$$\hat{\mathbf{W}}^{(0)} = M^{-1}\hat{\mathbf{r}}^{(0)} = M^{-1}\begin{pmatrix} \frac{A}{i} \\ \frac{A}{2i} \\ 0 \end{pmatrix}\delta(\alpha - \omega) - M^{-1}\begin{pmatrix} \frac{A}{i} \\ \frac{A}{2i} \\ 0 \end{pmatrix}\delta(\alpha + \omega).$$

Now taking the inverse Fourier transform on both sides gives

$$\mathbf{W}^{(0)} = M(\omega)^{-1}\begin{pmatrix} \frac{A}{i} \\ \frac{A}{2i} \\ 0 \end{pmatrix}e^{i\omega\tau} + M(-\omega)^{-1}\begin{pmatrix} -\frac{A}{i} \\ -\frac{A}{2i} \\ 0 \end{pmatrix}e^{-i\omega\tau}. \tag{28}$$

From (26)—i.e., from the definition of M—we know that

$$M(-\omega) = M(\omega)^*.$$

Therefore, if we define the vector $\mathbf{B}$ by

$$\mathbf{B} = M(\omega)^{-1}\begin{pmatrix} \frac{A}{i} \\ \frac{A}{2i} \\ 0 \end{pmatrix},$$

then (28) becomes

$$\mathbf{W}^{(0)} = \mathbf{B}e^{i\omega\tau} + \text{c.c.} \tag{29}$$

We have successfully obtained $\mathbf{W}^{(0)}$. It is now possible to iterate this procedure to determine $\mathbf{W}^{(1)}$ and to keep iterating until the approximation

$$\sum_{k=0}^{\mathcal{N}} b^k \mathbf{W}^{(k)}(\tau)$$

yields a sufficiently good approximation to the true steady-state solution of (22). With this in mind, we present the following algorithm for determining an approximation that is correct to order $b^{\mathcal{N}}\mathbf{W}^{(\mathcal{N})}$:

(b) *Algorithm 1.* For each k from 1 to $\mathcal{N}$, repeat the following steps. Assume that $\mathbf{W}^{(0)}, \mathbf{W}^{(1)}, \ldots, \mathbf{W}^{(k-1)}$ are already known. We determine the $O(b^k)$ term $\mathbf{W}^{(k)}$ as follows.

Step 1. Substitute $\mathbf{W}^{(0)}, \ldots, \mathbf{W}^{(k-1)}$ into the right-hand side of (22) and collect those terms with the coefficient b^k. Call these terms $\mathbf{r}^{(k)}$.

Note that, in general, one will have a set of real frequencies $\{\omega_1, \omega_2, \ldots, \omega_P\}$ and a set of complex vectors $\{\mathbf{s}_1, \mathbf{s}_2, \ldots, \mathbf{s}_P\}$ such that

$$\mathbf{r}^{(k)} = \sum_{j=1}^{P} (\mathbf{s}_j e^{i\omega_j\tau} + \mathbf{s}_j^* e^{-i\omega_j\tau}).$$

(Note that the integer P, the real frequencies $\{\omega_j\}_{j=1}^P$, and the complex vectors $\{\mathbf{s}_j\}_{j=1}^P$ will be different for each iteration of this algorithm.)

Step 2. Compute the Fourier transform $\hat{\mathbf{r}}^{(k)}$. In general, this will be

$$\hat{\mathbf{r}}^{(k)} = \sum_{j=1}^{P} [\mathbf{s}_j \delta(\alpha - \omega_j) + \mathbf{s}_j^* \delta(\alpha + \omega_j)],$$

where α is Fourier conjugate to τ.

Step 3. Now solve the linear system $M(\alpha)\hat{\mathbf{W}}^{(k)} = \hat{\mathbf{r}}^{(k)}$—i.e., write

$$\hat{\mathbf{W}}^{(k)} = M(\alpha)^{-1}\hat{\mathbf{r}}^{(k)} = \sum_{j=1}^{P} M(\alpha)^{-1}\mathbf{s}_j \delta(\alpha - \omega_j) + M(-\alpha)^{-1}\mathbf{s}_j^* \delta(\alpha + \omega_j).$$

Step 4. Finally, take the inverse Fourier transform of both sides to obtain

$$\mathbf{W}^{(k)} = \sum_{j=1}^{P} M(\omega_j)^{-1}\mathbf{s}_j e^{i\omega_j\tau} + M(-\omega_j)^{-1}\mathbf{s}_j^* e^{-i\omega_j\tau}.$$

Since $M(-\omega_j) = M(\omega_j)^*$, we see that the previous line can be rewritten as

$$\mathbf{W}^{(k)}(\tau) = \sum_{j=1}^{P} M(\omega_j)^{-1}\mathbf{s}_j e^{i\omega_j\tau} + \text{c.c.}$$

We have implemented Algorithm 1 in Mathematica and used it to generate an approximation to fourth order in b. Let us denote the W_R component of the Mathematica-generated approximation by W_R^{mm}:

$$W_R^{\text{mm}} = \sum_{k=0}^{4} b^k W^{(k)}(\tau) = B_R e^{i\omega\tau} + bC_R e^{2i\omega\tau} + b^2(D_{R,1}e^{3i\omega\tau} + D_{R,2}e^{i\omega\tau}) + b^3(E_{R,1}e^{4i\omega\tau} + E_{R,2}e^{2i\omega\tau}) + b^4(F_{R,1}e^{5i\omega\tau} + F_{R,2}e^{3i\omega\tau} + F_{R,3}e^{i\omega\tau}). \tag{30}$$

Our Mathematica implementation does provide analytical expressions for the coefficients B_R, C_R, $D_{R,j}$, $E_{R,j}$, and $F_{R,j}$. We omit these expressions for reasons of space.

F. Numerics for the 2×2 lattice

We again use numerical tests to justify the analysis done above. First we numerically solve (21) with saturating capacitance $C(v)$ given by (2) and input forcing $V(t) = A \sin t$. As before, we take $L=1$, $C_0=1$, $b=0.25$, $R=1$, and $A=0.3$. Once again this implies $\tau=t$, $\omega=1$, and $K=1$. We run the simulation from $\tau=0$ to $\tau=14\pi$. Let us denote the numerical solution for the voltage across the output resistor by $W_R^{\text{num}}(\tau)$. This function is plotted as the solid black curve in Fig. 10. The dash-dotted curve is the perturbative steady-state solution $W_R^{\text{mm}}(\tau)$ given by (30). It is clear that $W_R^{\text{num}}(\tau)$ reaches steady-state very quickly; for $\tau \geq 2\pi$, after just one period of input forcing, there is no discernable transient behavior, and both the dash-dotted and solid curves agree extremely well.

G. Interpretation

Just as we found for the 1×1 lattice, Algorithm 1 shows that going from the $O(b^k)$ approximation to the $O(b^{k+1})$ approximation results in the addition of higher harmonics to the output of the 2×2 lattice. The boundary excitation at frequency ω, interacting with the nonlinearity of the medium, kicks up output frequencies of 2ω, 3ω, 4ω, etc. We claim that these higher harmonics have larger amplitudes in the 2×2 case than they did in the 1×1 case.

To show that this is true, we again use a direct numerical simulation of (21) and the perturbative approximation (30) to plot the maximum output amplitude A_R as a function of the input amplitude A for the case where $\omega=1$ and $K=1$. We study the effect of two different nonlinearity values $b=0.05$ and $b=0.25$, which in Fig. 11 are shown in the left and right panels, respectively. Using the perturbative approximation (30), define

$$A_R = \max_{\tau\in[0,2\pi]} |W_R^{\text{mm}}(\tau)|.$$

The output A_R is shown as the dash-dotted black curve in both panels of Fig. 11.

We also generate numerical solutions $W_R^{\text{num}}(\tau)$ of the system (21) with saturating capacitance $C(v)$ given by (2) and

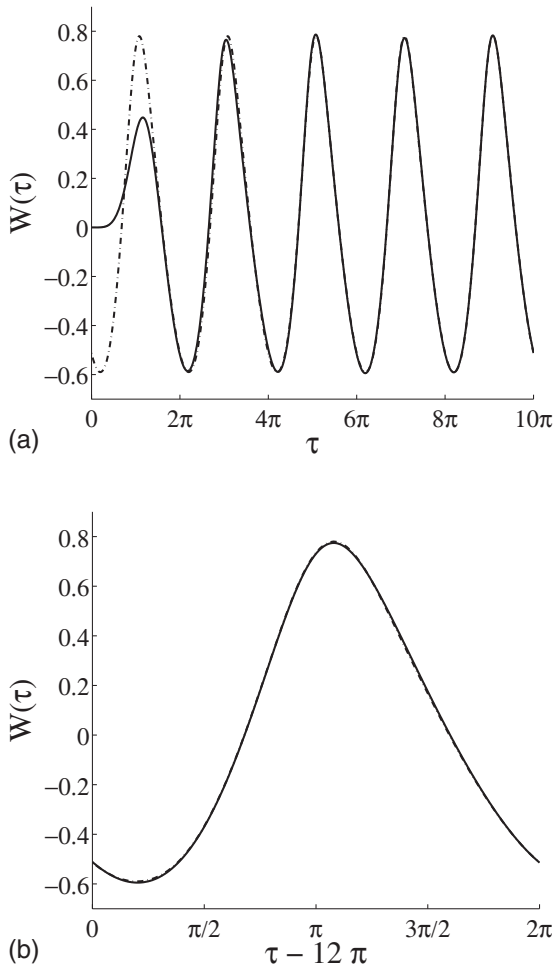

FIG. 10. The solid curve gives the numerical output voltage $W_R^{\text{num}}(\tau)$ generated by solving (21) with saturating capacitance $C(v)$ given by (2) and input forcing $V(t)=A \sin t$. The dashed curve is the perturbative solution $W_R^{\text{pmm}}(\tau)$ from (30). The left panel shows both solutions for $0 \leq \tau \leq 10\pi$, and the right panel shows both solutions for $12\pi \leq \tau \leq 14\pi$. Note from the left panel that the numerical solution reaches steady state very quickly and that both solutions become indistinguishable as τ increases from 2π. Both numerical and perturbative solutions have the same parameters $A=0.3$, $\omega=1$, $K=1$, and $b=0.25$.

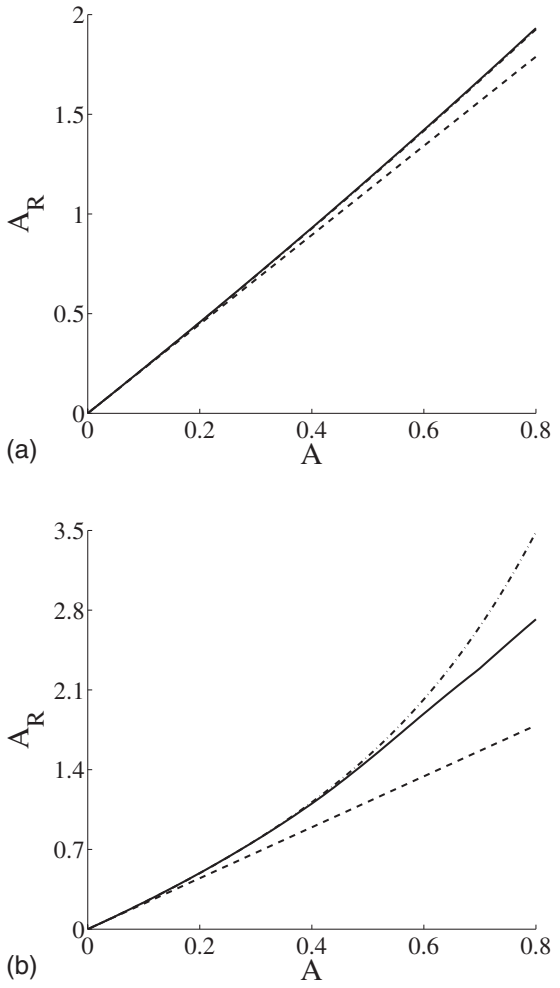

FIG. 11. There are three curves plotted in both panels. The lower dashed curve is the steady-state output amplitude for the $b=0$ linear lattice. The solid (numerical) and dash-dotted (fourth-order perturbative) upper curves give the steady-state nonlinear amplitudes for the two indicated values of b. Note that when $b=0.25$ and $A=0.4$, the nonlinear peak amplitude is roughly 23% higher than the linear peak amplitude. We set $K=1$ and $\omega=1$ for all runs.

input forcing $V(t)=A \sin t$ for values of A in the range $0 \leq A \leq 0.8$. We solve for $W_R^{\text{num}}(\tau)$ on the interval $0 \leq \tau \leq 14\pi$ with the parameters $\omega=1$, $K=1$, and either $b=0.05$ (left panel) or $b=0.25$ (right panel). We then compute the maximum output amplitude after the numerical solution has reached steady state—i.e.,

$$A_R^{\text{num}} = \max_{\tau \in [10\pi, 14\pi]} |W_R^{\text{num}}(\tau)|.$$

This is shown as the solid black curve in both panels of Fig. 11. In the left panel, where $b=0.05$, the solid black curve and dash-dotted black curve agree so closely that they are right on top of one another. When we increase the nonlinearity to $b=0.25$, as in the right panel, the two curves agree very closely except in the range $0.6 < A < 0.8$. In this range, as shown by the numerical simulations (solid curve), the output voltage A_R is sufficiently high that capacitor saturation has become an issue. The perturbative solution (dash-dotted curve) uses the nonsaturating $C_0(1-2bv)$ model. For $b=0.25$, this model is invalid for $v>2$; this is why in Fig. 11(b), when $A_R>2$, the perturbative solution overestimates the output voltage.

In both panels, we also plot (using a dashed line) the maximum amplitude that would have been observed had we set $b=0$—i.e., if we had a linear system with constant capacitors. As in the 1×1 case, we see from Fig. 11 that the linear $b=0$ response lies strictly below the $b>0$ curves.

In the middle of the graph, when $A=0.4$, we have that $A_R=1.1142$ and $A_R^{\text{num}}=1.1024$. The linear response to this input has amplitude 0.8944. That is to say, for an input signal with amplitude $A=0.4$, the higher harmonics in the nonlinear $b=0.25$ response provide a total amplitude boost of roughly 23% over the linear response.

Increasing the size of the lattice increases the amplitude of the higher harmonics, thereby *strengthening* the nonlinear

constructive interference and leading to a larger relative boost over the linear response.

IV. GENERALIZATION TO $N\times N$ LATTICES

A. Amplitude boost

We have enough information to begin to understand how the voltage dependence of the capacitors in an 80×80 lattice can cause a large increase in amplitude, as shown in Fig. 4. In what follows, we assume that all lattice parameters are the same as those used to produce Fig. 4. In particular, we assume that $b=0.25$ and that the input forcing is applied to the last 20 nodes on the left boundary and the first 20 nodes on the bottom boundary. Our explanation of Fig. 4 is as follows.

(i) After $\tau=2\pi$, the nonlinear 2×2 system has already reached steady state. We extrapolate from this that a large subblock would reach steady state at $\tau=8\pi$, which is the time at which the data in Fig. 4 were taken. Even if the dynamics of the rest of the lattice has not yet reached steady state, as long as the input amplitudes are not small, the transient dynamics does not display significant overshoot or undershoot. The steady-state theory remains a useful guide.

(ii) Our analytical and numerical steady-state calculations indicate that increasing the size of the lattice from 1×1 to 2×2 can increase the relative amplitude gain (over the linear $b=0$ lattice) from 8% to 23%. From this result, we expect that the output amplitude for a 20×20 nonlinear lattice can be several multiples of the linear output.

(iii) However, the numerics for the 2×2 lattice indicates that capacitor saturation decreases the relative amplitude boost. The upshot is that once the output voltage has saturated the capacitors, increasing the lattice size (and thereby adding more voltage-dependent capacitors) yields diminishing returns.

(iv) The steady-state analytical calculations from the previous section indicate that the mechanism behind this amplitude boost is constructive interference of higher harmonics. That is, if the input consists of $e^{i\omega t}$, the output can be approximated by

$$\sum_{k=1}^{\mathcal{N}} c_k b^k e^{ik\omega t},$$

for complex coefficients $c_1,\ldots,c_{\mathcal{N}}$. Given the input amplitude A, we solved for the coefficients c_k by iterating an equation of the form $M(\alpha)\hat{\mathbf{W}}^{(k)}=\hat{\mathbf{r}}^{(k)}$. In the 1×1 case, this matrix $M(\alpha)$ was a 1×1 matrix:

$$M(\alpha)=-\alpha^2+iK\alpha+2.$$

In the 2×2 case, the matrix $M(\alpha)$ is given by (26). For the 20×20 case, as we show later in this paper, the steady-state solution will again involve iteration of the equation $M(\alpha)\hat{\mathbf{W}}^{(k)}=\hat{\mathbf{r}}^{(k)}$, where the matrix $M(\alpha)$ is now 210×210. We conjecture that the inversion of this much larger matrix leads to much larger coefficients $\hat{\mathbf{W}}^{(k)}$.

We conclude that nonlinear constructive interference can be used to obtain large output voltages A_R, even if this results in an arbitrarily large ratio A_R/A of the output amplitude to input amplitude. In other words, there is nothing special about the peak at approximately $A\approx 0.60$ in Fig. 4(b)—a voltage-dependent capacitor that saturates at a higher voltage would allow an even higher ratio of A_R/A.

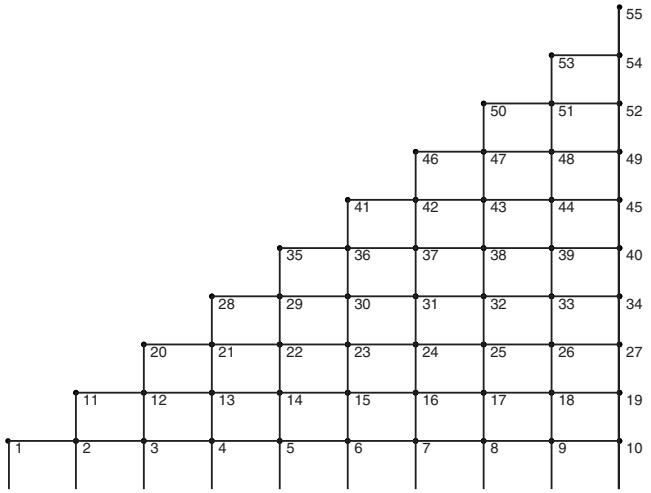

FIG. 12. Symmetry-reduced 10×10 lattice.

B. Theory

We now generalize the results of Sec. III E, including Algorithm 1, to the case of an $N\times N$ lattice. As before, we assume that the inputs along the left and bottom boundaries are equal-amplitude and in-phase inputs. This means that the voltages and currents above the diagonal can be deduced by symmetry—i.e., by reflection across the diagonal. Taking advantage of this symmetry, we may consider an equivalent lattice with only $J=N(N+1)/2$ voltage unknowns. Note that we have already used this symmetry in the 2×2 case to pass from Fig. 9(a) to Fig. 9(b), which has $2(2+1)/2=3$ unknown voltages.

We present a graph of the symmetry-reduced $N=10$ inductor-capacitor lattice in Fig. 12. In Fig. 12, edges correspond to inductors, through which we have unknown currents. Nodes correspond to voltage-dependent capacitors (connected to ground), across which we have unknown voltages.

Note that the nodes are numbered left to right, bottom to top, from 1 to $10(11)/2=55$. Nodes 1 through N each have one edge that connects the node to a prescribed voltage source, $V_{\text{in}}(t)$; see Figs. 5 and 9. As in those diagrams, we treat node 1 as connected to two voltage sources and we treat the upper-right node J [where, again, $J=N(N+1)/2$] as connected to a resistor R.

Having numbered the nodes, we can now construct the $J\times J$ matrix $M(\alpha)$ that generalizes (26). We plan to carry out this construction without writing down Kirchhoff's laws throughout the lattice. Instead, we argue as follows. Suppose we have an infinite square lattice. Labeling the nodes as in Fig. 2, we obtain Kirchhoff's laws in the form of system (1) where i and j can be arbitrary integers.

Differentiating (1a) with respect to t and then using (1b) and (1c) to eliminate the current variables from the right-hand side, we find that

$$L\frac{d^2}{dt^2}[Q(V_{i,j})] = -4V_{i,j} + V_{i+1,j} + V_{i-1,j} + V_{i,j+1} + V_{i,j-1} = (\delta^2 V)_{ij}, \tag{31}$$

where the right-hand side denotes the discrete Laplacian of V on the infinite rectangular lattice, evaluated at (i,j). Let

$$\sigma_{p,q} = \begin{cases} 0, & p \neq q, \\ 1, & p = q. \end{cases}$$

Let us ignore capacitor saturation and again set $C(v)=C_0(1-2bv)$ and $Q(v)=C_0(v-bv^2)$. Then, by analogy with (31), we claim that for the lattice diagrammed in Fig. 12, at each node j, we will have a second-order equation

$$LC_0\frac{d^2}{dt^2}[V_j - bV_j^2] = (\delta^2 V)_j - \frac{\sigma_{j,J}}{R}\frac{d}{dt}V_J + 2\sigma_{j,1}V_{\text{in}}(t) + \sum_{k=2}^{N}\sigma_{j,k}V_{\text{in}}(t). \tag{32}$$

To complete (32), we must describe how to compute $(\delta^2 V)_j$, the discrete Laplacian of V on the finite lattice diagrammed in Fig. 12, evaluated at node j. We make the following three definitions.

(i) Let ξ_j denote the number of edges that are directly connected to node j.

(ii) Let $\zeta_j(k)=1$ if node k is precisely one edge away from node j, and let $\zeta_j(k)=0$ otherwise.

(iii) Let $\lambda_j=2$ if node j is on the diagonal—i.e., if there exists m such that $j=1+mN-m(m-1)/2$. Let $\lambda_j=1$ otherwise.

With these definitions, we may express the discrete Laplacian by

$$(\delta^2 V)_j = \lambda_j\left(-\xi_j V_j + \sum_{k=1}^{J}\zeta_j(k)V_k\right). \tag{33}$$

Substituting (33) into (32), we have

$$LC_0\frac{d^2}{dt^2}[V_j - bV_j^2] = -\lambda_j\xi_j V_j + \lambda_j\sum_{k=1}^{J}\zeta_j(k)V_k - \frac{\sigma_{j,J}}{R}\frac{d}{dt}V_J + 2\sigma_{j,1}V_{\text{in}}(t) + \sum_{k=2}^{N}\sigma_{j,k}V_{\text{in}}(t). \tag{34}$$

This system of second-order equations, from $j=1$ to $j=J$, is the generalization of (21) to the $N\times N$ case. From here onwards, we follow the same steps as before. We switch to the nondimensionalized time $\tau=t/\sqrt{LC_0}$ and define $K=\sqrt{L/C_0}/R$. We set $V_j(t)=W_j(\tau)$ and $V_{\text{in}}(t)=S(\tau)$. Then (34) becomes

$$W_j'' + \sigma_{j,J}KW_J' + \lambda_j\xi_j W_j - \lambda_j\sum_{k=1}^{J}\zeta_j(k)W_k = 2bW_jW_j'' + 2b(W_j')^2 + 2\sigma_{j,1}S(\tau) + \sum_{k=2}^{N}\sigma_{j,k}S(\tau). \tag{35}$$

We expand $W_j(\tau)$ in a series:

$$W_j(\tau) = W_j^{(0)}(\tau) + bW_j^{(1)}(\tau) + b^2W_j^{(2)}(\tau) + \cdots. \tag{36}$$

Substituting (36) into (34), we obtain, at zeroth order in b,

$$\frac{d^2}{d\tau^2}W_j^{(0)} + \sigma_{j,J}K\frac{d}{d\tau}W_J^{(0)} + \lambda_j\xi_j W_j^{(0)} - \lambda_j\sum_{k=1}^{J}\zeta_j(k)W_k^{(0)} = 2\sigma_{j,1}S(\tau) + \sum_{k=2}^{N}\sigma_{j,k}S(\tau). \tag{37}$$

Define $\mathbf{r}^{(0)}:\mathbb{R}\to\mathbb{R}^J$, a vector-valued function of τ, as follows:

$$\mathbf{r}^{(0)}(\tau) = \mathbf{h}S(\tau),$$

with $\mathbf{h}=(2,\underbrace{1,\ldots,1}_{N-1},\underbrace{0,\ldots,0}_{J-N})^T$. As before, we take the Fourier transform on both sides of (37) with α as the Fourier conjugate to τ. The result is

$$M(\alpha)\hat{\mathbf{W}}^{(0)} = \hat{\mathbf{r}}^{(0)}. \tag{38}$$

Here $\mathbf{W}=(W_1,\ldots,W_J)^T$, $\hat{\mathbf{W}}$ is the Fourier transform of $\mathbf{W}$, and $M(\alpha)$ is a $J\times J$ matrix that may be constructed as follows.

(i) Start with a $J\times J$ zero matrix. For each row j from 1 to J, proceed column by column. Put -1 in column k if and only if node k is precisely one edge away from node j—i.e., if $\zeta_j(k)=1$. For column j, put ξ_j, the total number of edges directly connected to node j. The final matrix is symmetric by construction.

(ii) Take the matrix from the previous step. For each row j from 1 to J, multiply the row by 2 if node j is a node on the diagonal—i.e., if $\lambda_j=2$. Otherwise do nothing to row j.

(iii) Subtract α^2 from the diagonal.

(iv) Add $iK\alpha$ to the lower-right corner.

(c) *Obtaining* $\mathbf{W}^{(0)}$ for single-frequency forcing. Take $S(\tau)=A\sin\omega\tau$, so that

$$\hat{\mathbf{r}}^{(0)} = \mathbf{h}\left(\frac{A}{2i}\delta(\alpha-\omega) - \frac{A}{2i}\delta(\alpha+\omega)\right).$$

Then by (38) we find that

$$\hat{\mathbf{W}}^{(0)} = (M(\alpha)^{-1}\mathbf{h})\left(\frac{A}{2i}\delta(\alpha-\omega) - \frac{A}{2i}\delta(\alpha+\omega)\right). \tag{39}$$

Taking the inverse Fourier transform of both sides gives

$$\mathbf{W}^{(0)}(\tau) = M(\omega)^{-1}\mathbf{h}\frac{A}{2i}e^{i\omega\tau} - M(-\omega)^{-1}\mathbf{h}\frac{A}{2i}e^{-i\omega\tau}.$$

Since $M(-\omega)=M(\omega)^*$, we can rewrite this last equation as

$$\mathbf{W}^{(0)}(\tau) = \mathbf{B}e^{i\omega\tau} + \text{c.c.},$$

with

$$\mathbf{B} = M(\omega)^{-1}\mathbf{h}\frac{A}{2i}.$$

(d) *Algorithm 1, reexamined.* Now that we have constructed $M(\alpha)$ and solved for $\mathbf{W}^{(0)}$, we can reapply almost all of Algorithm 1 to solve for the successively higher approximations $\mathbf{W}^{(k)}$ for $k=1,2,\ldots,\mathcal{N}$. The only part of the algorithm that must be changed is the construction of the right-hand side vector $\mathbf{r}^{(k)}$, i.e., step 1 of Algorithm 1. In the $N\times N$ case, the revised version of step 1 reads as follows.

Step 1'. Substitute $\mathbf{W}^{(0)},\ldots,\mathbf{W}^{(k-1)}$ into the right-hand side of (34) and collect those terms with the coefficient b^k. Call these terms $\mathbf{r}^{(k)}$.

The note following step 1 and all of steps 2, 3, and 4 still apply. This gives a general algorithm for finding a perturbative approximation to the steady-state response of an $N\times N$ lattice to single-frequency forcing along the left and bottom boundaries.

(e) *Future work.* The version of Algorithm 1 for $N\times N$ lattices suggests a concrete problem whose solution would yield an analytical model of Fig. 4. Namely, one can attempt to derive estimates on the matrix norm of the $J\times J$ matrix $M(\alpha)$, as a function of α and J. These estimates would enable one to estimate the size of $\hat{\mathbf{W}}^{(k)}$ for successively larger values of k, which could then be used to estimate the steady-state output amplitude for a large nonlinear lattice. To correctly solve for large steady-state amplitudes, one must modify our perturbative calculations to take into account capacitor saturation. Both of these tasks require extensive mathematical analysis and are outside the scope of the current work.

V. CONCLUSION

A. Relationship to Kadomtsev and Petviashvili

In an $N\times N$ lattice, there are N^2 unknown voltages and $2N^2$ unknown currents, for a total of $3N^2$ degrees of freedom. Unfortunately, the theory of nonlinear dynamical systems does not cope well with finite-dimensional systems in $\mathbb{R}^N$ with $N\gg 10$. One way to proceed is to model the finite-dimensional system by an infinite-dimensional system obtained from a continuum limit.

In prior work [1], we applied the method of reductive perturbation theory to (1a)–(1c) and showed that in a weakly nonlinear continuum limit, lattice voltage is governed by the negative-dispersion Kadomtsev-Petviashvili (KP) equation:

$$[V_t + VV_x + V_{xxx}]_x + V_{yy} = 0. \tag{40}$$

The KP equation has exact soliton solutions, and it is completely integrable by the inverse scattering method [17]. Moreover, the KP equation has exact solutions that consist of two incoming solitons of amplitude A and one outgoing soliton with amplitude at most $4A$ [18]. In the literature, this process is sometimes called soliton resonance [19,20]. A recent paper [21] shows how the symmetries of KP may be utilized to characterize large classes of resonant soliton solutions. For such solutions to exist, n input solitons must collide at precise angles, yielding m output solitons with predetermined phase shifts and amplitudes.

While it is interesting that the KP equation has exact solutions that correspond to our notion of nonlinear constructive interference, such solutions do not explain Fig. 4. As Fig. 4 indicates, by changing the amplitude of the inputs, we can tune the ratio A_R/A. It is not fixed at 4, as it would be for a corresponding soliton resonance solution of KP. Resonant solutions of KP consist of colliding solitons, while in our lattice the waves that collide are formed from harmonic forcing of the boundary. Furthermore, we have carried out numerical experiments that show that nonlinear constructive interference in LC lattices occurs for a range of collision angles, not just one precise angle.

We interpret the complete integrability and infinite number of symmetries of the KP equation as *constraints* on nonlinear wave collisions. Driving and damping at the boundary are intrinsic aspects of our problem. If we model a damped, driven lattice using the same weakly nonlinear limit as in [1], we obtain an equation that consists of KP equation (40) plus extra, symmetry-breaking, nonconservative terms. Our conjecture is that breaking the integrability of the KP equation allows for a much more diverse array of nonlinear collisions.

B. Lattice cutoff frequency

The present work demonstrates that nonlinear constructive interference is possible in two-dimensional, bounded, nonlinear electrical lattices. Such lattices can be built on chip and the interference phenomena can be used for a variety of applications. The applications we have in mind involve input signals with frequency content that exceeds the cutoff frequency of the fastest active components—e.g., transistors. In the linear $b=0$ case, the lattice equations reduce to

$$V_{i,j-1} - 2V_{i,j} + V_{i,j+1} + V_{i-1,j} - 2V_{i,j} + V_{i+1,j} = LC\frac{d^2}{dt^2}V_{ij}. \tag{41}$$

By considering plane-wave propagation with wave vector $\mathbf{k}=(k_x,k_y)$ and frequency f, one finds the dispersion relation

$$4\pi^2 f^2 = \frac{2}{LC}[2 - (\cos k_x + \cos k_y)]. \tag{42}$$

Clearly the maximum value of f occurs when $k_x=k_y=\pm\pi$. In this case,

$$f_M = \frac{1}{2\pi}\sqrt{\frac{8}{LC}}. \tag{43}$$

With state-of-the-art integrated-circuit technologies on a silicon substrate, the minimum possible integrated inductance and capacitance are, approximately, $L_M=30$ pH and $C_M=5$ fF. Below these values, parasitic inductance and capacitance dominate. Using these values in (43), we find that the maximum frequency for plane-wave propagation on a 2D silicon transmission lattice is $f_M\approx 1.16$ THz. Waves with frequency that approach this cutoff will occupy a small num-

ber of lattice spacings. The physical wavelength λ will be very small.

Though the preceding analysis is exact only for linear lattices, it is clear that an analysis of general inductor-capacitor lattices for frequencies close to the cutoff will involve waves where the A/λ ratio is large and the λ/h ratio is small. This is a regime where the asymptotics described earlier, and therefore the KP equation itself, does not apply. This is another reason why, in our analysis, we worked with the lattice ordinary differential equations (1a)–(1c) directly, rather than with the KP equation or with any other continuum model.

ACKNOWLEDGMENTS

The authors thank B. Deconinck, J. N. Kutz, and B. Osting for discussions regarding various aspects of this work. H.S.B. was partially supported by NSF Grant No. DMS-0753983. E.A. was partially supported by NSF Grant No. DMS-0713732.

[1] E. Afshari, H. S. Bhat, A. Hajimiri, and J. E. Marsden, J. Appl. Phys. **99**, 054901 (2006).
[2] E. Afshari, H. S. Bhat, X. Li, and A. Hajimiri, in *Proceedings of the IEEE International Solid-State Circuits Conference, San Francisco, 2006*, edited by L. C. Fujino (IEEE, New York, 2006), pp. 206–208.
[3] E. Afshari, H. S. Bhat, and A. Hajimiri, IEEE Trans. Circ. Syst. I (to be published).
[4] G. Friesecke and K. Matthies, Discrete Contin. Dyn. Syst. **3**, 105 (2003).
[5] M. Feckan and V. M. Rothos, Nonlinearity **20**, 319 (2007).
[6] I. A. Butt and J. A. D. Wattis, J. Phys. A **39**, 4955 (2006).
[7] I. A. Butt and J. A. D. Wattis, J. Phys. A **40**, 1239 (2007).
[8] J. C. Eilbeck, P. S. Lomdahl, and A. C. Newell, Phys. Lett. **87A**, 1 (1981).
[9] A. R. Bishop and P. S. Lomdahl, Physica D **18**, 54 (1986).
[10] P. S. Lomdahl and M. R. Samuelsen, Phys. Rev. A **34**, 664 (1986).
[11] Y. S. Kivshar and B. A. Malomed, Rev. Mod. Phys. **61**, 763 (1989).
[12] S. Watanabe, H. S. J. van der Zant, S. H. Strogatz, and T. P. Orlando, Physica D **97**, 429 (1996).
[13] B. A. Malomed, Phys. Rev. B **49**, 5962 (1994).
[14] J. L. Marin and S. Aubry, Nonlinearity **9**, 1501 (1996).
[15] A. Vanossi, K. O. Rasmussen, A. R. Bishop, B. A. Malomed, and V. Bortolani, Phys. Rev. E **62**, 7353 (2000).
[16] B. Hu and J.-Y. Zhu, Phys. Rev. E **65**, 016202 (2001).
[17] A. C. Newell, *Solitons in Mathematics and Physics*, Regional Conference Series in Applied Mathematics, Vol. 48 (SIAM, Philadelphia, 1985).
[18] E. Infeld and G. Rowlands, *Nonlinear Waves, Solitons and Chaos*, 2nd ed. (Cambridge University Press, Cambridge, 2000).
[19] J. W. Miles, J. Fluid Mech. **79**, 157 (1977).
[20] J. W. Miles, J. Fluid Mech. **79**, 171 (1977).
[21] G. Biondini and Y. Kodama, J. Phys. A **36**, 10519 (2003).